Proceedings of the International Conference on Aerospace System Science and Engineering 2020
ICASSE2020
July 14-16, 2020, Shanghai, China

Navigation Information Augmented Artificial Potential Field Algorithm for Collision Avoidance in UAV Formation Flight

Huahua Liu[1,2], Hugh H. T. Liu[2], Cheng Chi[1], Yawei Zhai[1], Xingqun Zhan[1*]
1. School of Aeronautics and Astronautics, Shanghai Jiao Tong University, Shanghai, China
2. University of Toronto Institute for Aerospace Studies, Toronto, Canada
*Corresponding Author, E-mail: xqzhan@sjtu.edu.cn

Abstract: In recent years, multiple Unmanned Aerial Vehicle (UAV) formation flight has attracted worldwide research interest, for its potential benefits of scalability and flexibility. In complex urban environments, the successful operation of those UAVs requires the system to provide certain safety level. As one of the key requirements, collision avoidance improves the system's ability to accommodate operational environment variations, and to perform multiple tasks. To achieve this, Artificial Potential Field (APF) has been recognized as one of the most suitable methods along with drone control and motion planning. In particular, it holds great promise for applications in unknown environments. Although there has been substantial relevant work on the APF algorithm for single UAV in static environment, more efforts are desired to address formation maneuvers in complex environments such as urban. Most importantly, traditional APF algorithms do not account for random errors in navigation solutions, which can bring potential risk to the UAV system. In response, this paper proposes a new APF algorithm that employs navigation information in complex urban environments, and the goal is to realize UAV formation collision avoidance. By augmenting the APF algorithm with UAV navigation information, the potential risk caused by navigation uncertainty can be mitigated, especially in the Global Navigation Satellite System (GNSS) challenged environment. The principle of the new approach is adaptively estimating the parameters of potential field force function, using the variance of navigation information and user-defined confidence probability. Besides, the corresponding Linear Quadratic Regulator (LQR) controller is adopted to apply the formation motion synchronization control and to combine with the new approach with high efficiency. As a result, the drones can achieve fast position and attitude adjustment with high safety confidence. To verify the algorithm, quadrotors with emulated GNSS receivers are used to generate observation data. These data are incorporated into a complex urban environment simulation, where multiple sets of virtual obstacles are injected. Results show that the proposed method can achieve safe and effective collision avoidance for cooperative formation flight in urban GNSS challenged environment.

Keywords: *unmanned aerial vehicle; artificial potential field; collision avoidance; formation control; Global Navigation Satellite System*

1 Introduction

Unmanned Aerial Vehicle (UAV) formation operation in urban environment is an emerging technological development with a significant potential market. It has been extensively researched in recent years from the perspective of formation control, navigation, collision avoidance et al. And the intended applications of UAV formation flight include payload delivery, emergency response, environmental monitoring in urban environments [1]. However, there exists a need

to address the challenge of multiple obstacles and the poor data quality of the Global Navigation Satellite System (GNSS) in environments where the GNSS is degraded due to the urban canyon effect. Accordingly, as for the navigation aspect, the unreliability of navigation performance in urban should be considered [2]. Meanwhile, the control of UAVs is a major area of interest, drones need to move stably with high efficiency and avoid obstacles.

Multi-UAV cooperative control, as a prerequisite for efficient completion of various tasks, has always been an important subject for urban UAV research. It employs certain strategies to make drones form a specific structure without collision. Comparing to single UAV scenario, the formation improves the system's robustness against operational environment changes and covers a larger operation area. Regarding an urban environment in complex situation, multiple UAVs can take advantage of formations to extend the scope of operations and mitigate interference of the UAV state judgement. This helps to improve the system's environmental adaptability and expand the efficiency of task execution, enhance the reliability, and significantly expand the application range of drones [3].

Formation movements can be treated as a multi-UAV system with a fixed configuration during the flight [4]. The formation control technologies mainly include Leader-Follower method, Behavior-based method and Virtual Structure method [5]. Leader-follower control is one of the most popular formation control strategies for its easy implementation [6]. Cledat [7] proposed a coordinated leader-follower mapping based on two drones, which kept one drone flying high enough to receive Global Positioning System (GPS) signals and to provide indirect position control for the second drone. In this way, the automatic navigation and acquisition of aerial images in a GPS-restricted environment are realized, but this may lead to a serious accident when the position of the leader drone becomes lost. However, the virtual structure method can avoid this failure, as the entire formation is regarded as a rigid body structure. After years of development, many researchers have made great contributions to this topic. Nevertheless, there are still some drawbacks to be solved. For example, in the method utilized in [8] to maintain the formation geometry, it can effectively achieve formation control but the results failed to account for formation synchronization error. Besides, the application ranges of virtual structure formation flight control are mainly in formation air mobility without obstacle avoidance requirements. As in [9], two UAVs adopted the configuration of the classic virtual structure method and applied motion synchronous. It improved the robustness of formation control and the maintenance of the formation configuration, but it only considered a simple situation without obstacles.

However, UAV operations in urban require the system to achieve urban air mobility while avoiding obstacles. Collision avoidance has always been an active issue of UAV control research, and it is a precondition to realize safe operations over various tasks [10]. The collision avoidance means that the mobile drone moves along the trajectory in an environment with obstacles, and safely avoid the collision according to specific operating rules [10]. The most widely studied local collision avoidance algorithms are neural network algorithm, fuzzy logic algorithm, Artificial Potential Field (APF) algorithm, genetic algorithm, etc. [11]. Among them, the APF algorithm is a high-efficiency algorithm with simple structure and smooth path, which is suitable for solving the problem of collision avoidance in the unknown environment with a large number of objects [12]. Initially, the APF method was proposed by Khatib [13]. Researches in APF algorithm for single UAV flying in a static environment have been quite mature, and current researches focus on complex environments such as urban environments. Recently, LYU Yong-shen et al [14] combined the virtual structure method with APF to achieve formation flight. Despite this, far too little attention of APF algorithm has been paid to the impact of uncertainty of navigation information in GNSS degraded environment, which can bring potential risk to the UAV system. The objective of this paper is to investigate a Navigation Information Augmented APF (NAPF) collision avoidance formation motion synchronization method which accounts for the uncertainty of navigation information in various environments. The velocity related APF function is modified to combine the variances of navigation states. Moreover, the motion

synchronization technology is integrated into the virtual structure formation control to improve the performance of formation controllers and maintenance of the formation geometry. Simulations were presented with four UAVs and different numbers of obstacles. By taking 30-times Monte-Carlo simulations, the proposed algorithm shows a significant reduction in collision probability.

In this paper, Section 2 introduces the unmanned aerial vehicle formation motion synchronization with corresponding LQR controller to form a square formation. Section 3 firstly presents the traditional APF algorithm for UAVs collision avoidance, and then proposes the NAPF algorithm to reduce the Collision Risk (CR) of the UAV formation. Section 4 presents the simulations and results. Section 5 concludes this work.

2 Cooperative Virtual Structure Formation

The formation movement of multi-UAV requires multiple mobile agents to fly along a certain path while maintaining the defined formation configuration during the movement.

2.1 UAV modeling

Simplification of quadrotor control modeling has greatly been adopted to make the model more applicable [15][16], and the derived state-space model chosen consists of twelve corresponding state vector and the input vector can be represented as follows,

$$\chi^T = \left[x, \dot{x}, y, \dot{y}, z, \dot{z}, \phi, \dot{\phi}, \theta, \dot{\theta}, \psi, \dot{\psi} \right] \tag{1}$$

$$u^T = \left[F_z, \tau_\phi, \tau_\theta, \tau_\psi \right] \tag{2}$$

$$\begin{cases} F_i = k_i \ \Omega_i^2 \\ \tau_i = k_d \ \Omega_i^2 \end{cases} \qquad for \quad i = 1, .. 4 \tag{3}$$

$$\begin{cases} F_x = & 0 \\ F_y = & 0 \\ F_z = & -\left(F_1 + F_2 + F_3 + F_4\right) \\ \tau_\phi = & l\left(F_4 - F_2\right) \\ \tau_\theta = & l\left(F_1 - F_3\right) \\ \tau_\psi = & \tau_1 - \tau_2 + \tau_3 - \tau_4 \end{cases} \tag{4}$$

where $\left(x, y, z\right) \in R^3$ represents the displacement and $\left(\phi, \theta, \psi\right) \in R^3$ is the attitude angle in the inertial frame, l represents the distance between the geometric center of the UAV and motor center, F_i and τ_i denote the thrust force and the moments of attitude, respectively. Ω represents the angular speed of UAV propellers.

And the UAV state-space model can be presented as Eq. (5), which is presented in terms of multiple second-order nonlinear descriptions,

$$\begin{bmatrix} \dot{x} \\ \ddot{x} \\ \dot{y} \\ \ddot{y} \\ \dot{z} \\ \ddot{z} \\ \dot{\phi} \\ \ddot{\phi} \\ \dot{\theta} \\ \ddot{\theta} \\ \dot{\psi} \\ \ddot{\psi} \end{bmatrix} = \begin{bmatrix} \dot{x} \\ 0 \\ \dot{y} \\ 0 \\ \dot{z} \\ -g \\ \dot{\phi} \\ \dot{\theta}\dot{\psi}\dfrac{\left(I_y - I_z\right)}{I_x} + \dfrac{\dot{\theta}J}{I_y}\Omega \\ \dot{\theta} \\ \dfrac{\dot{\psi}\dot{\phi}\left(I_z - I_x\right) + \dot{\phi}J\Omega}{I_y} \\ \dot{\psi} \\ \dfrac{\dot{\theta}\dot{\phi}\left(I_x - I_y\right)}{I_z} \end{bmatrix} + \begin{bmatrix} 0 & 0 & 0 & 0 \\ \dfrac{\left(\cos\dot{\phi}\sin\dot{\theta} + \sin\dot{\phi}\sin\dot{\psi}\right)}{m} & 0 & 0 & 0 \\ 0 & \cdot & \cdot & \cdot \\ \dfrac{\left(\cos\dot{\phi}\sin\dot{\theta}\sin\dot{\psi} - \sin\dot{\phi}\cos\dot{\psi}\right)}{m} & \cdot & \cdot & \cdot \\ 0 & \cdot & \cdot & \cdot \\ \dfrac{\cos\dot{\theta}\cos\dot{\phi}}{m} & 0 & 0 & 0 \\ 0 & 0 & 0 & 0 \\ 0 & \dfrac{1}{I_x} & 0 & 0 \\ \cdot & 0 & 0 & 0 \\ \cdot & 0 & \dfrac{1}{I_y} & 0 \\ \cdot & 0 & 0 & 0 \\ 0 & 0 & 0 & \dfrac{1}{I_z} \end{bmatrix} \begin{bmatrix} u_1 \\ u_2 \\ u_3 \\ u_4 \end{bmatrix} \tag{5}$$

Then the model needs to be linearized on the basic of the nonlinear dynamic equations of motion expression to make it more applicable to control. According to the equilibrium $\dot{\bar{\chi}} = 0$,

$$\phi_2 = \theta_2 = \psi_2 = 0 \tag{6}$$

and take it into account that UAV is required to moves along a given trajectory with the desired heading angle, and thus obtaining the equilibrium point,

$$\begin{cases} \bar{u}_1 = b\left(\Omega_1^2 + \Omega_2^2 + \Omega_3^2 + \Omega_4^2\right) = mg \\ \bar{u}_2 = lb\left(\Omega_4^2 - \Omega_2^2\right) = 0 \\ \bar{u}_3 = lb\left(\Omega_3^2 - \Omega_3^2\right) = 0 \\ \bar{u}_4 = d\left(\Omega_2^2 + \Omega_4^2 - \Omega_3^2 - \Omega_1^2\right) = 0 \end{cases} \tag{7}$$

$$\bar{\chi} = \begin{pmatrix} \bar{x}_1 & 0 & \bar{y}_1 & 0 & \bar{z}_1 & 0 & 0 & 0 & 0 & 0 & \bar{\psi}_1 & 0 \end{pmatrix} \tag{8}$$

$$\bar{U} = \begin{pmatrix} \bar{u}_1 & 0 & 0 & 0 \end{pmatrix}, \quad \bar{Y} = \begin{pmatrix} \bar{x}_1, \bar{y}_1, \bar{z}_1, \bar{\psi}_1 \end{pmatrix} \tag{9}$$

Then the following linearized UAV error dynamic equation based on the error vector set in Eq. (13) can be obtained,

$$\begin{cases} \dot{\tilde{\chi}} = A\tilde{\chi} + B\tilde{U} \\ Y = C\tilde{\chi} \end{cases} \tag{10}$$

$$\begin{cases} \tilde{\chi} = \chi - \bar{\chi} \\ \tilde{U} = U - \bar{U} \\ \tilde{Y} = Y - \bar{Y} \end{cases} \tag{11}$$

A Linear Quadratic Regulator (LQR) feedback controller $\tilde{U} = -\mathrm{K}\tilde{\chi}$ is adopted based on the linearized state-space model to converges error dynamically. By designing certain Q and R to construct state feedback control law K, which minimizes cost function J.

$$J = \frac{1}{2}\int_{t=0}^{\infty}\left(\tilde{\chi}^{\mathrm{T}}Q\tilde{\chi} + \tilde{U}^{\mathrm{T}}R\tilde{U}\right)dt \tag{12}$$

The state feedback control law can be obtained from the Riccati equation [9], and the optimal control law of LQR controller is,

$$U^{*}=-K^{*}\tilde{\chi}=-R^{-1}B^{T}\tilde{\chi} \tag{13}$$

2.2 Virtual Structure Formation Motion Synchronization

In order to maintain the UAV formation during air mobility and eliminate relative position errors, a cooperative formation control method based on virtual structure and motion synchronization is constructed. The cooperative formation controller generates reference commands to LQR controller to maintain the formation shape. The virtual structure method is applied to form a four UAV square formation. Through keeping each drone away with a certain distance from the hypothetical point, a certain formation geometric configuration is maintained. And the geometric center of the formation is chosen as the virtual point in this paper. The synchronization control of formation can be transformed into the stabilization of error variables.

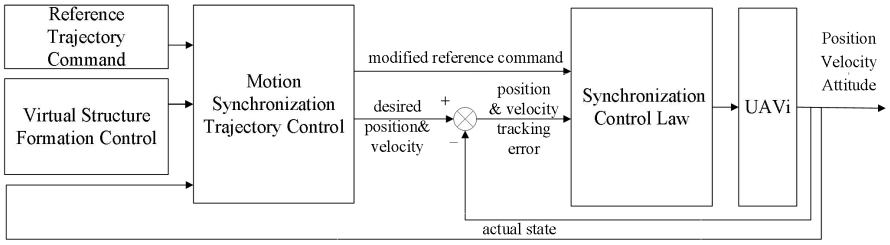

Fig. 1. Virtual Structure Formation Synchronization Structure

The overall proposed formation cooperative flight control method is shown in Fig. 1. The formation controller takes the formation synchronization error, the reference trajectory instruction based on reference waypoint $P=(x_r,y_r,z_r)$ and the actual position $X=(x,y,z)$ of UAV as inputs. The motion synchronization concept is utilized to modify the relative position of the synchronized formation tracking trajectory [17].

$$\begin{cases} e_p=\left(1-nn^{T}\right)\left(X-P_{r0}\right) \\ e_v=\bar{V}-nV=\dot{X}-nV \end{cases} \tag{14}$$

where e_v and e_p are the error vector of velocity and position, respectively. P_{r0} is the start position reference path n is the direction of UAV air mobility $n^{T}n=1$ and the direction of the reference velocity V_r can be represented as $\bar{V}_r^{d}=nV_r$ [18].

The configuration of the four drone formations is constructed as square geometric. The four UAVs take off from any different initial position and stabilize with the defined geometric configuration at a given starting point. And then, UAVs begin to synchronize the formation movement.

As shown in Fig. 2, for the convenience of computation, we define $u=np'\times\left(P-X\right)$ as the position of UAV projections on the reference path. s represents the side length of the square geometric configuration. Then we can acquire the start point of the other two UAVs according to the set start point of UAV1 and UAV2.

$$\begin{cases} p_{4y}=p_{1y}+s\sin\beta \\ p_{3y}=p_{2y}-s\sin\beta \end{cases} \tag{15}$$

$$\begin{cases} \alpha = \arcsin \dfrac{p_{1y} - p_{2y}}{\sqrt{2}s} \\ \beta = \dfrac{\pi}{4} - \alpha \end{cases} \tag{16}$$

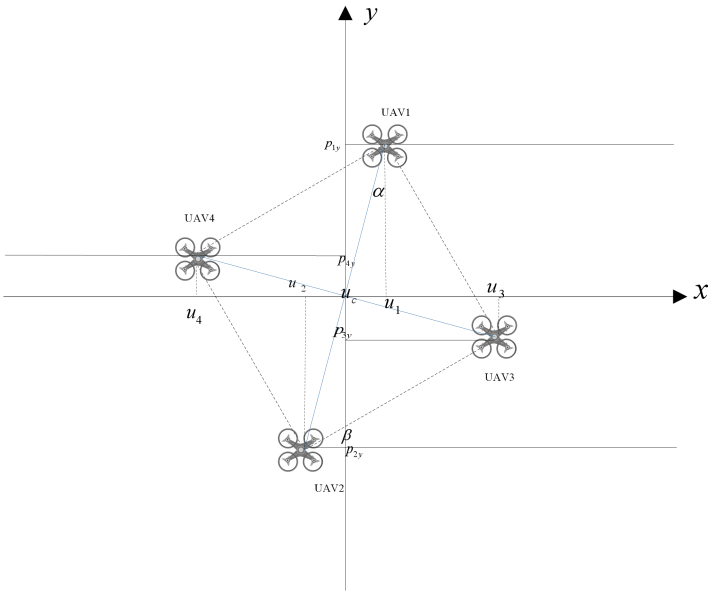

Fig. 2. Square virtual structure cooperative formation top view configuration

l_1 to l_4, which are the distance between the center reference point and the projection of each UAV, can be defined as follows,

$$\begin{cases} l_1 = u_1 - u_c = \dfrac{s}{\sqrt{2}} \cos\alpha \\ l_2 = u_c - u_2 = \dfrac{s}{\sqrt{2}} \cos\alpha \\ l_3 = u_3 - u_c = \dfrac{s}{\sqrt{2}} \sin\alpha \\ l_4 = u_c - u_4 \dfrac{s}{\sqrt{2}} \sin\alpha \end{cases} \tag{17}$$

where the center reference point of the square formation $u_c = \dfrac{1}{4}(u_1 + u_2 + u_3 + u_4)$ is calculated according to the position of four UAVs.

The desired position of each UAV and formation synchronization error ef_i during flight is obtained according to the reference point and the relative distance between UAVs defined in the virtual structure formation control method.

$$\begin{cases} ef_1 = u_1 - (u_c + l_1) \\ ef_2 = u_2 - (u_c + l_2) \\ ef_3 = u_3 - (u_c + l_3) \\ ef_4 = u_4 - (u_c + l_4) \end{cases} \tag{18}$$

$$\begin{cases} V_{r1} = V_r + k_f \cdot ef_1 \\ V_{r2} = V_r + k_f \cdot ef_2 \\ V_{r3} = V_r + k_f \cdot ef_3 \\ V_{r4} = V_r + k_f \cdot ef_4 \end{cases} \tag{19}$$

The formation synchronization tracking error of the aircraft is fed back to the synchronization module. The trajectory controller generates a modified trajectory command for each drone according to the formation error. These synchronization errors are mixed with the tracking errors of velocity and position, which is the final error signal input to the synchronization formation controller. And then, the controller continuously eliminates relative errors to maintain the square formation geometry effectively during flight. The control law is presented as,

$$\begin{aligned} f_i &= -k_p\left(1-nn^T\right)\left(X_i-P_i\right)-k_v\left(\dot{X}_{\mathrm{i}}-nV\right) \\ &= -k_p\left(1-nn^T\right)\left(X_i-P_i\right)-k_v\left(\dot{X}_{\mathrm{i}}-n\left(V_{\mathrm{r}}+k_f\cdot ef_i\right)\right) \\ &= -k_v\left(\dot{X}_{\mathrm{i}}-nV_r\right)-k_p\left(1-nn^T\right)X_i-k_p\left(1-nn^T\right)P_i+k_vk_fn\cdot ef_i \\ &= -k_v\left(\dot{X}_{\mathrm{i}}-nV_r\right)-k_p\left(1-nn^T\right)\left(X_i-P_i\right)+k_vk_fn\cdot ef_i \end{aligned} \tag{20}$$

As we define the $\tilde{V}$ and $\tilde{r}$ represent the tracking error vector of position and velocity, respectively.

$$\begin{cases} \tilde{V}_i=\vec{V}_i-\vec{V}_d=\dot{X}_{\mathrm{i}}-nV_r=\vec{V}_i-nV_r \\ \tilde{r}_i=r_i-r_d=X_i-P_i \end{cases} \tag{21}$$

The control law consists of synchronization error and the tracking error vector of position and velocity can be described as,

$$f_i=-k_v\tilde{V}_i-k_p\left(1-nn^T\right)\tilde{r}_i+k_vk_fn\cdot ef_i \tag{22}$$

The goal of the square formation motion synchronization is to gradually converge error of each drone to zero, which means that tracking error and synchronization error are both driven to 0. That is, UAVs utilize each other's information to eliminate errors synchronously. Accordingly, each UAV is integrated with the other UAVs in the square formation, which effectively maintains the formation geometry and achieve formation motion synchronization.

3 APF Formation collision avoidance

In the process of urban formation air mobility, it is highly imperative to not only maintain a stable formation but also to consider obstacles in the environment throughout the entire flight of the formation system. Since each drone needs to avoid collision during flight according to a certain strategy like APF.

3.1 APF collision avoidance Algorithm

The APF algorithm has a wide range of applications in drone obstacle avoidance path planning because of its simple principle, simple structure and smooth generation path. The method does not need to search the global path, has short planning time and high execution efficiency, and is very suitable for real-time and security requirements for collision avoidance [22]. The basic principle is to regard the drone flying in a virtual artificial force field, in which the target point generates an attractive force to the drone and the obstacles generate repulsion to the drone. When the potential field composing of the repulsive and attractive potential field is applied, the drone flies along the direction in which the APF descends to search for the collision-free optimal path. The resultant force of attraction and repulsion is utilized as the acceleration force for the mobile agent to control the direction of drone mobility and to calculate the position of the drone [23]. The drone constantly adjusts its attitude, velocity, and direction according to the detected information including the distance between the obstacle and the drone, the state of obstacles. The purpose is to guide the drone to avoid obstacles while moving to the target point under the potential energy field.

The APF can be regarded as the energy field. The drone always moves from the direction of high potential energy to the low potential energy, attracting the drone to the target point and being rejected by the obstacle.

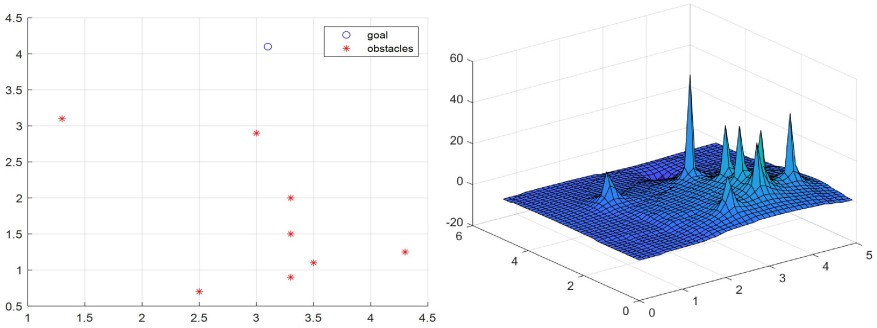

Fig. 3. Potential field distribution map according to goal and obstacles set

To illustrate the basic principles of the potential field, we simulated its distribution based on the goal and the set obstacle, which is shown in Fig. 3. It is clear that the attractive potential field of the APF method gradually decreases as the drone approaches the target point, and the goal is the minimum point of the potential field, and the repulsive field increases when it gets closer to the obstacles.

The repulsive function is correlated with the distance between UAV and obstacle. As the distance between obstacle and drone decreases, the repulsive potential increases. By the time the repulsive potential energy of the drone becomes 0, it means that this mobile drone has left the influence limit of the obstacles. Artificial Repulsion from the Surface function (FIRAS) function is applied as the repulsive potential field function $U_{rep}(X)$,

$$U_{rep}(X)=\begin{cases}\dfrac{1}{2}k_r\left(\dfrac{1}{\rho(X,X_o)}-\dfrac{1}{\rho_0}\right)^2, & \rho(X,X_o)\le\rho_0\\ 0, \rho(X,X_o)\ge\rho_0\end{cases} \tag{23}$$

where k_r is the repulsive gain factor. $X=(x,y,z)^T$ and $X_o=(x_o,y_o,z_o)^T$ are the position vector of UAV and obstacle, respectively. $\rho(X,X_o)$ denotes a vector and the magnitude of it denotes the Euclidean distance between the UAV and obstacle,

$$\rho(X,X_o)=\|X_o-X\| \tag{24}$$

There are often multiple obstacles in the space when the UAV moves along the trajectory. If the repulsion of each obstacle to the UAV is considered despite some obstacle are far from the drone, the UAV collision avoidance may fail due to too many computations. In order to reduce the unnecessary calculations of the UAV obstacle avoidance and ensure the safety of UAV, the collision avoidance boundary should be set and ρ_0 represents the safety distance [20].

The drone can be pulled from the starting point to the goal by the attractive potential field. The endpoint of the attractive field is the global minimum point of the entire APF, which is the goal that the UAV needs to reach. The attractive potential field is set to be proportional to the distance between the UAV and goal $\rho(X,X_g)$. The characteristics of this potential field are similar to elastic potential energy so attractive potential field function can be expressed as,

$$U_{att}(X)=\frac{1}{2}k_a\rho^2(X,X_g) \tag{25}$$

where k_a represents the attractive gain factor and $\rho\left(X, X_g\right)$ represents the vector of distance between the position of the UAV X and the goal X_g.

$$\rho\left(X, X_g\right) = \left\| X_g - X \right\| \tag{26}$$

The force exerted on the drone is a negative gradient of the APF function,

$$F_{att} = -\nabla\left[U_{att}\left(X\right)\right] = k\rho\left(X, X_g\right) \tag{27}$$

$$F_{rep} = -\nabla\left[U_{rep}\left(X\right)\right] = \begin{cases} k\left(\dfrac{1}{\rho\left(X, X_o\right)} - \dfrac{1}{\rho_0}\right)\dfrac{1}{\rho^2\left(X, X_0\right)}\dfrac{\partial_\rho}{\partial_x}, \rho\left(X, X_o\right) \le \rho_0 \\ 0, \rho\left(X, X_o\right) \ge \rho_0 \end{cases} \tag{28}$$

where F_{att} is the corresponding attraction and F_{rep} is the corresponding repulsion. Then the resultant force $F\left(X\right)$ is expressed as follow,

$$F\left(X\right) = F_{att}\left(X\right) + F_{rep}\left(X\right) \tag{29}$$

The mathematical principle is used to analyze the force magnitude and direction of the drone.

$$\alpha = \arctan\frac{y_g - y}{x_g - x} \tag{30}$$

$$\begin{cases} F_{att}\left(x\right) = F_{att}\cos\left(\alpha\right) \\ F_{att}\left(y\right) = F_{att}\sin\left(\alpha\right) \end{cases} \tag{31}$$

Supposing the number of the obstacles is n and the angle between the UAV and obstacles and the components of the repulsion force function can be expressed as,

$$\begin{aligned} \beta_{o1} &= \arctan\frac{y_{o1} - y}{x_{o1} - x} \\ \beta_{o2} &= \arctan\frac{y_{o2} - y}{x_{o2} - x} \\ &\vdots \\ \beta_{on} &= \arctan\frac{y_{on} - y}{x_{on} - x} \end{aligned} \tag{32}$$

$$\begin{cases} F_{rep}\left(x\right) = F_{rep}\cos\left(\beta_{oi}\right) \\ F_{rep}\left(y\right) = F_{rep}\sin\left(\beta_{oi}\right) \end{cases} \tag{33}$$

The resultant force angle can reflect the direction state of the resultant force in real-time. At this time, the virtual force control for the traditional APF can be converted into angle control.

$$\theta = \frac{F\left(y\right)}{F\left(x\right)} = \frac{F_{att}\left(y\right) + F_{rep}\left(y\right)_1 + F_{rep}\left(y\right)_2 + \cdots + F_{rep}\left(y\right)_n}{F_{att}\left(x\right) + F_{rep}\left(x\right)_1 + F_{rep}\left(x\right)_2 + \cdots + F_{rep}\left(x\right)_n} \tag{34}$$

And the next position of UAV can be calculated according to,

$$\begin{cases} x_{i+1} = x_i + \gamma\cos\theta_i \\ y_{i+1} = y_i + \gamma\sin\theta_i \end{cases} \tag{35}$$

The drone moves from $\left(x_i, y_i\right)$ to $\left(x_{i+1}, y_{i+1}\right)$ as the current position point and sets $i = i + 1$ as the current state. The entire motion planning process is an

iterative update of the mobility control, and the position of the mobile drone at the current time is determined by the resultant force angle at the last moment.

It can be seen from the formula (34) that the calculation amount of the drone motion direction is proportional to the number of obstacles in the motion space. Thus, the time complexity of the drone collision avoidance is positively related to the number of obstacles in the operating environment. To combine with the formation synchronization motion more properly, we modified the APF algorithm into velocity update expression, which can reduce the complexity of calculation.

In term of the repulsive field and the attractive field defined in Eq. (23) and Eq. (25), the overall APF function can be obtained as follows,

$$U(X) = U_{att}(X) + \sum_i U^i_{rep}(X) \tag{36}$$

$$V_i = -\nabla U(X) + \overline{V}_i \tag{37}$$

$$\begin{cases} V_i = \sqrt{V_{xi}^2 + V_{yi}^2 + V_{zi}^2} \\ \theta_i = \arctan\left(\dfrac{V_{zi}}{V_{xi}}\right) \\ \psi_i = \arctan\left(\dfrac{V_{yi}}{V_{xi}}\right) \end{cases} \tag{38}$$

$$\begin{cases} \delta_i = \arctan\left(\dfrac{V_{xi}}{V_{yi}}\right) - \arctan\left(\dfrac{\overline{V}_{xi}}{\overline{V}_{yi}}\right), \quad \delta_i \in \left(-60/(180/\pi), 60/(180/\pi)\right) \\ n_{i+1} = \left(n_i + \cos\delta_i, n_i + \sin\delta_i\right) \\ n = \dfrac{n_{i+1}}{\|n_{i+1}\|} \end{cases} \tag{39}$$

where n represents the direction of i^{th} trajectory, δ represents the angle change of the UAV velocity and $V_i^d = nV_i$ shows the direction of UAV mobility.

The obstacle avoidance trajectory command $T_r = [P_i, n_i, V_i]$ can be updated according to Eq. (39). The entire collision avoidance process is an iterative update of the reference velocity. Compared with the traditional APF algorithm which directly decomposes the total potential field force as the control force to update the UAV position, this algorithm is realized by adjusting the velocity command of each drone, and the track instruction updates smoother and faster. If the distance between obstacles and UAVs is less than the safe distance, APF algorithm is applied to modify the command to avoid obstacles and the cooperative formation motion synchronization adopted to maintain the formation configuration.

3.2 Navigation Information Augmented Artificial Potential Field Algorithm

Regarding collision avoidance is an important part of formation safety in urban environments, a certain repulsive force is supposed to be generated by APF with certain safe distance to keep the mobile agent away, thereby avoiding the collision between the agents safely. The visibility of GNSS in the urban environment will affect the positioning error [24]. When UAVs fly in GNSS challenges the environment, the measurement error will change. When the distance between UAVs and obstacle is close, this positioning error will threaten their safety. Therefore, we reconstruct the potential field function parameters based on the variance provided by the navigation system, and then the controller can dynamically adjust the safety threshold based on the positioning error to reduce the impact of navigation information uncertainty on flight safety.

First, we determine the magnitude interval of the navigation positioning results, that is, the results of navigation positioning fall into a certain range according to a certain probability, this type of uncertainty estimation is called error interval estimation. If a navigation positioning value is x and the corresponding standard deviation is σ, assuming the error follows a normal distribution, the error interval can be estimated as $[x-k\sigma, x+k\sigma]$. When the $k=3$, the corresponding collision avoidance probability is 99.74%.

4 Simulations

In order to verify the effect of the constructed APF algorithm on the UAVs collision avoidance motion, a series of simulation experiments are carried out in the MATLAB environment. The main parameter values affect the method in the potential field formula based on the constructed algorithm are the attractive gain coefficient and repulsive potential field gain coefficient.

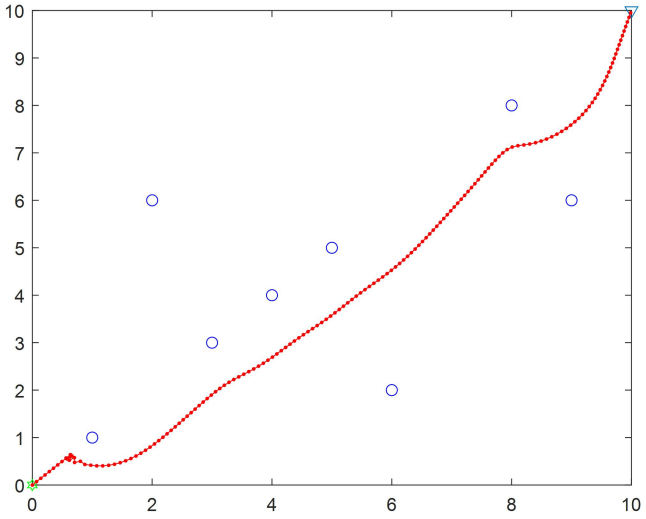

Fig. 4. APF collision avoidance algorithm of a single UAV

The collision avoidance algorithm of a single drone is verified in Fig. 4. In the simulation, the target point coordinate is set to (10, 10), the starting point coordinate is (0, 0), and the set obstacle be a circular obstacle with a radius of 1. The red dotted line in the figure shows the drone collision avoidance path, the target point is a triangle and the blue circles are obstacles. In the static obstacle environment, by adjusting the attractive $k_a = 2.5$ and repulsive gain coefficient $k_r = 15$, collision avoidance can be achieved effectively and smoothly and the simulation shows that the drone can successfully achieve collision avoidance with a safe and smooth collision avoidance path.

As the simulations are performed based on the four UAV virtual structure formation motion synchronization. The parameters of the UAV system are defined as follows: the weight of each UAV is 1kg, the moments of inertia along x, y, z axis are $I_x = I_y = 8.1\times10^{-3}$, $I_z = 14.2\times10^{-3}$, lift coefficient and drag coefficient are $b = 54.2\times10^{-6}$, $d = 4.2\times10^{-6}$. And the parameters of the reference path are set as follows: the initial positions and velocities of four UAV are $X_1=(0,-1,0)$, $X_2=(1,1,1)$, $X_3=(2,-1,0)$, $X_4=(0,2,0)$, $V_1=(0,0,0)$, $V_2=(1,1,1)$, $V_3=(2,2,0)$, $V_4=(1,0,1)$ and the square side length s=10m. Set the reference path start position of UAV1 and UAV2 $P_1=(0,3,0)$, $P_2=(0,-3,0)$. The direction of the i^{th} reference trajectory is $n=(1,0,0)$. $kf = -0.5$ and the weighting matrix Q and R of LQR controller are chosen as,

$$Q = 10^{-1} \times I_{12}, \quad R = \begin{bmatrix} 10^{-1} & 0 & 0 & 0 \\ 0 & 10 & 0 & 0 \\ 0 & 0 & 10^{2} & 0 \\ 0 & 0 & 0 & 10 \end{bmatrix}.$$

Then the simulations of APF obstacles avoidance of the four UAV formation are carried out by defining 8 obstacles around the set reference trajectory. The simulations of the four UAV square formation obstacle avoidance algorithm under the condition of 8 obstacles are shown in Fig. 5 - Fig. 8.

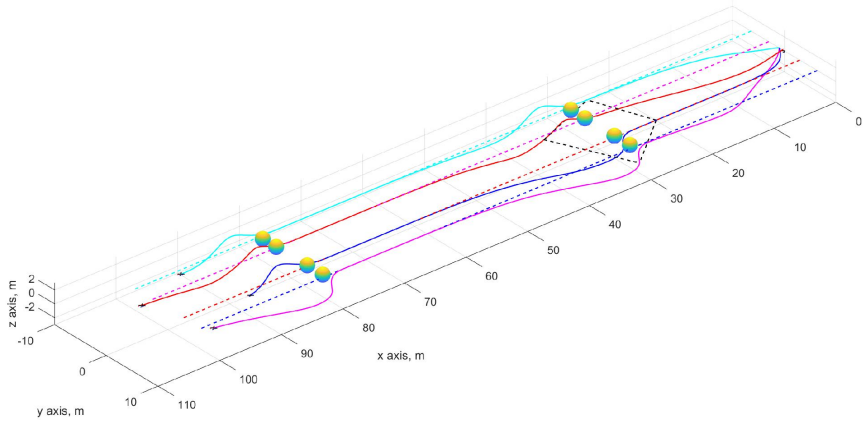

Fig. 5. The collision avoidance trajectory with 8 obstacles

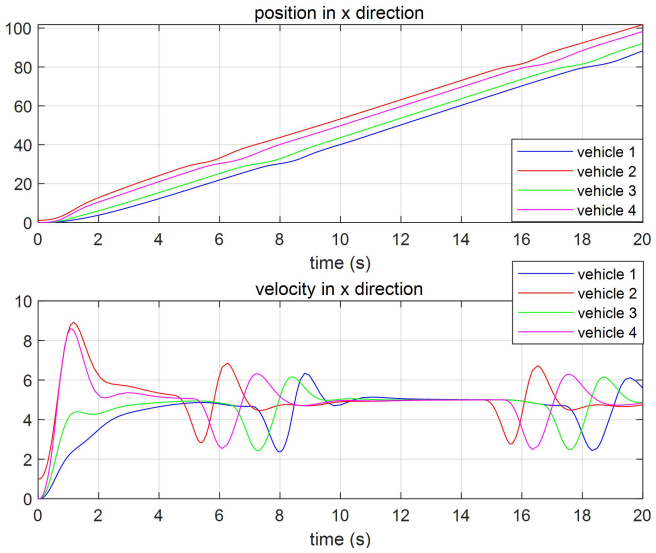

Fig. 6. x-direction position and velocity of 8 obstacles formation collision avoidance

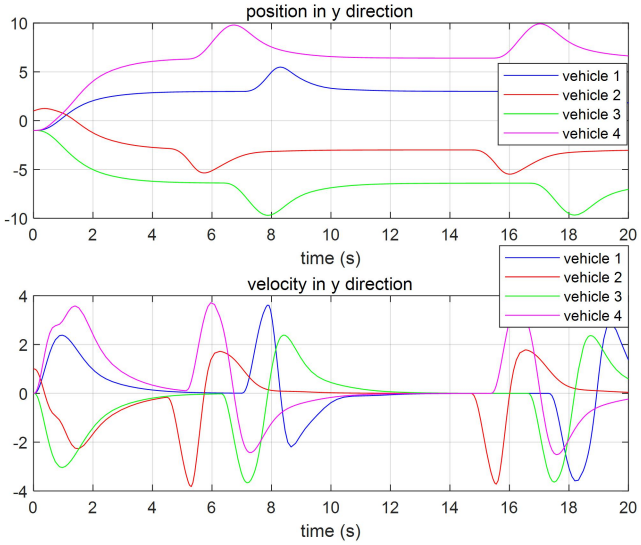

Fig. 7. y-direction position and velocity of 8 obstacles formation collision avoidance

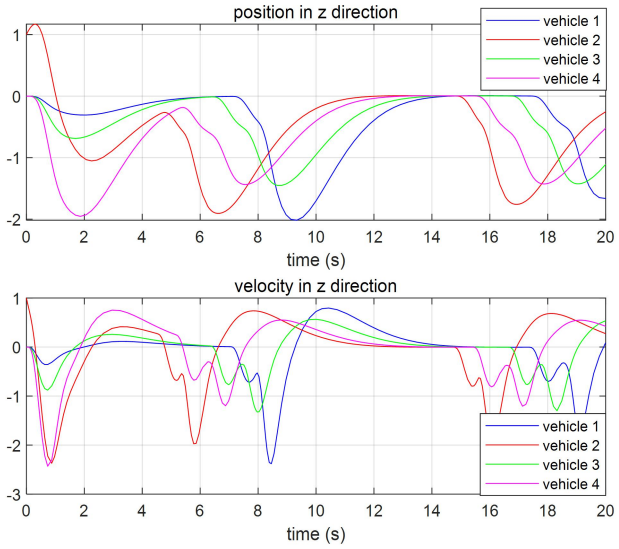

Fig. 8. z-direction position and velocity of 8 obstacles formation collision avoidance

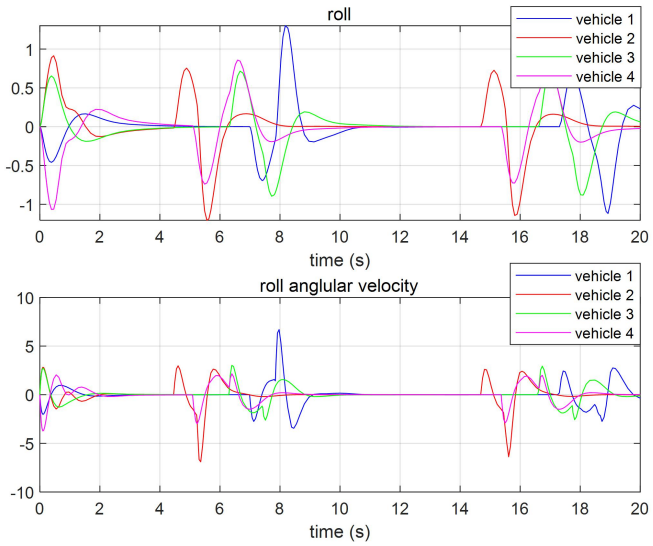

Fig. 9. Roll and roll angular velocity of 8 obstacles formation collision avoidance

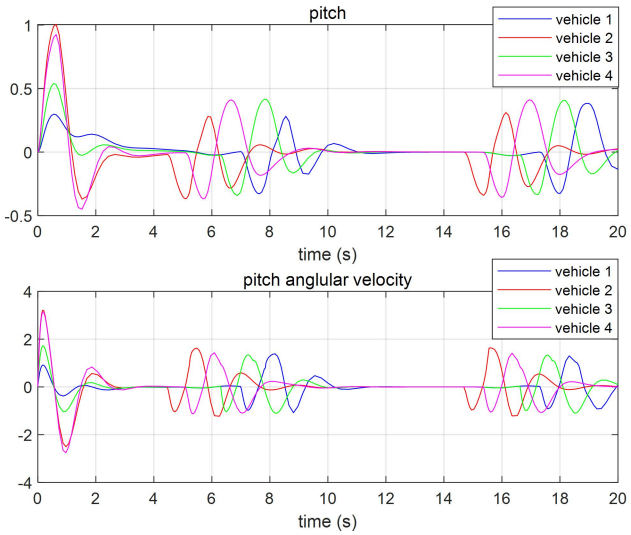

Fig. 10. Pitch and pitch angular velocity of 8 obstacles formation collision avoidance

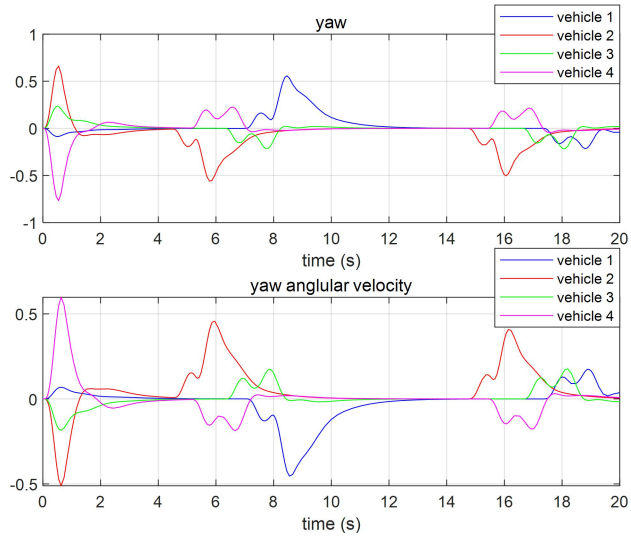

Fig. 11. Yaw and yaw angular velocity of 8 obstacles formation collision avoidance

It can be seen from Fig. 5 that the four drones can achieve obstacle avoidance formation flight. The curves in Fig. 6 - Fig. 11 verify that formation can achieve formation obstacle avoidance by quickly adjusting positions and attitudes when moving along the formation reference path toward the set direction. At the same time, after leaving the influence of obstacles, the formation is gradually reconfigured and maintains the formation structure effectively and stably under the control of the cooperative formation.

Next, to verify the effectiveness of APF formation collision avoidance algorithm in a more complex environment, we set 40 obstacles and the size and position of obstacles are randomly generated.

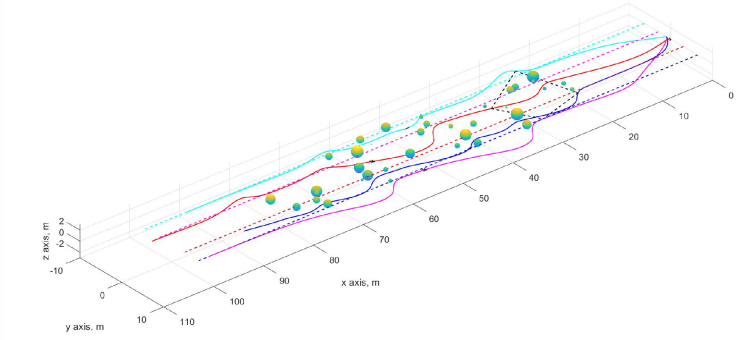

Fig. 12. The collision avoidance trajectory with 40 obstacles

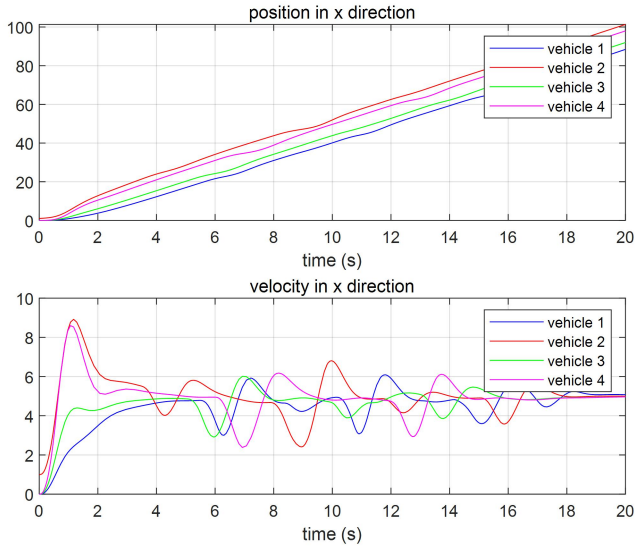

Fig. 13. x-direction position and velocity of 40 obstacles formation collision avoidance

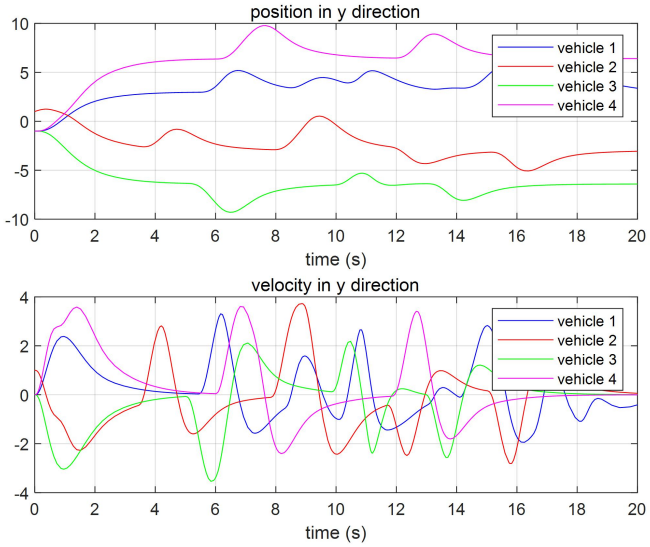

Fig. 14. y-direction position and velocity of 40 obstacles formation collision avoidance

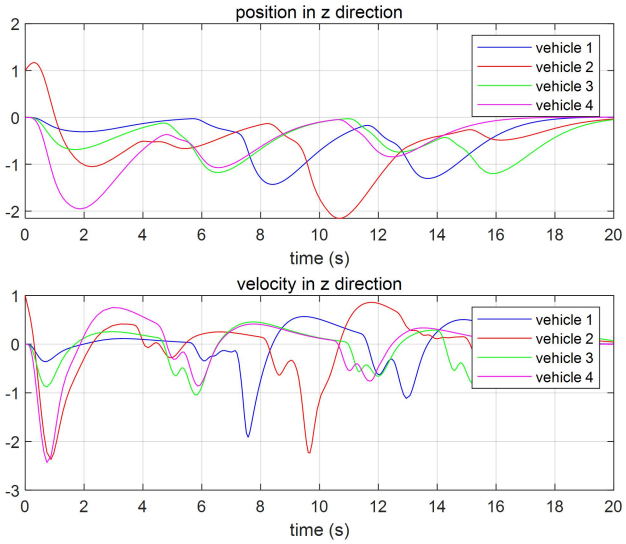

Fig. 15. z-direction position and velocity of 40 obstacles formation collision avoidance

The simulation of the four UAV square formation collision avoidance path under the condition of 40 obstacles is shown in Fig. 12. It can be seen from the Fig. 13 - Fig. 15 that after the obstacles increases, the four drones can also achieve

collision avoidance formation flight. However, compared with the 8 obstacles situation, this UAV collision avoidance path has a larger angle of steering when passing the area affected by dense obstacles.

In order to simulate the uncertainty of navigation information, dynamic positioning errors fluctuating between 1m and 5m are introduced in the actual track feedback *x*, *y*, *z* channels. The improved APF function changes the safety distance from the original fixed value to dynamically change according to the variance output of the simulated navigation filter.

Table 1. Collision risk of APF Algorithm

Algorithm	Collision risk
Original APF	73.33%
Navigation information enhanced APF	16.67%

Table 1 presents the comparison of collision risk between improved APF algorithm augmented with navigation information and original APF. After 30 times of simulations, the collision risk of improved APF square formation obstacle avoidance algorithm improved is reduced from 73.33% to 16.67%, which shows that the potential risk caused by navigation quality uncertainty can be mitigated.

Through the following simulations, the obstacles avoidance effects of the navigation information enhanced APF and the APF with a fixed safety distance in 8 and 40 obstacles environments are compared.

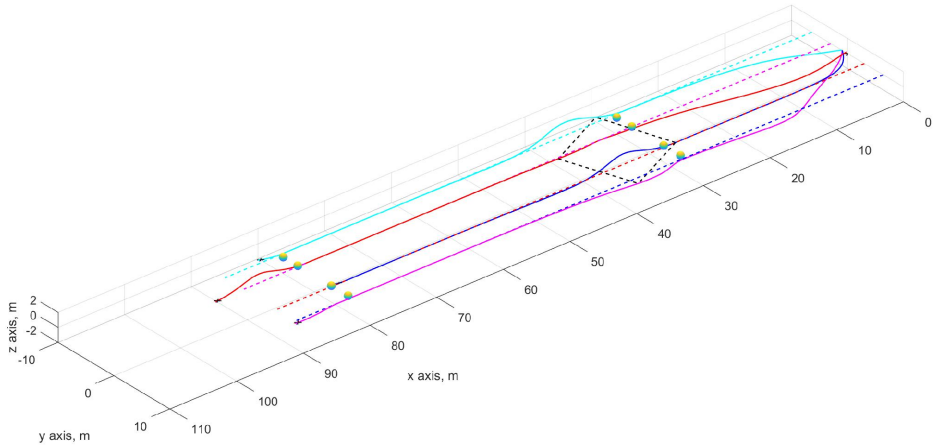

Fig. 16. The fixed safety distance APF collision avoidance trajectory with 8 obstacles

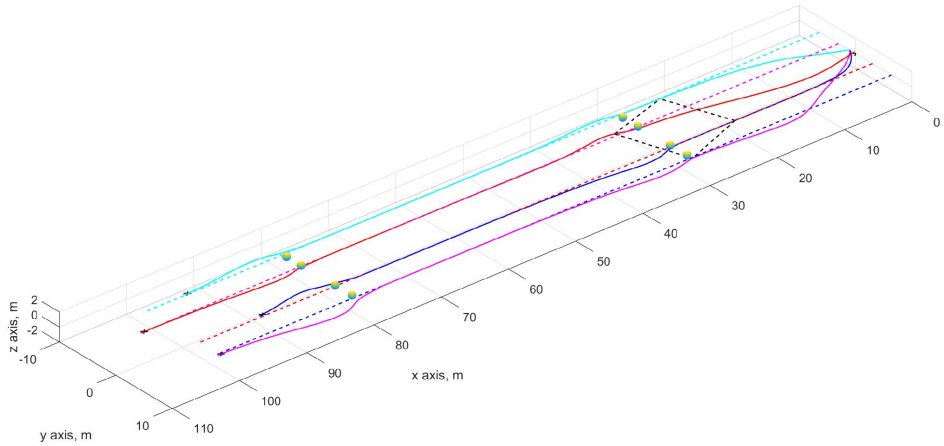

Fig. 17. The navigation information enhanced APF collision avoidance trajectory with 8 obstacles

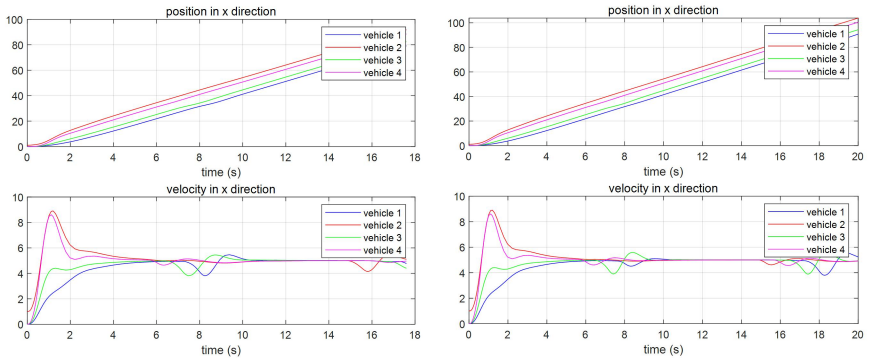

Fig. 18. x-direction position and velocity of original APF and navigation information enhanced APF 8 obstacles formation collision avoidance

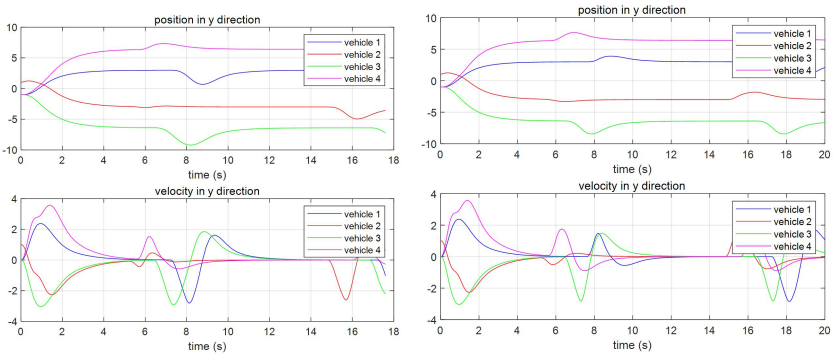

Fig. 19. y-direction position and velocity of original APF and navigation information enhanced APF 8 obstacles formation collision avoidance

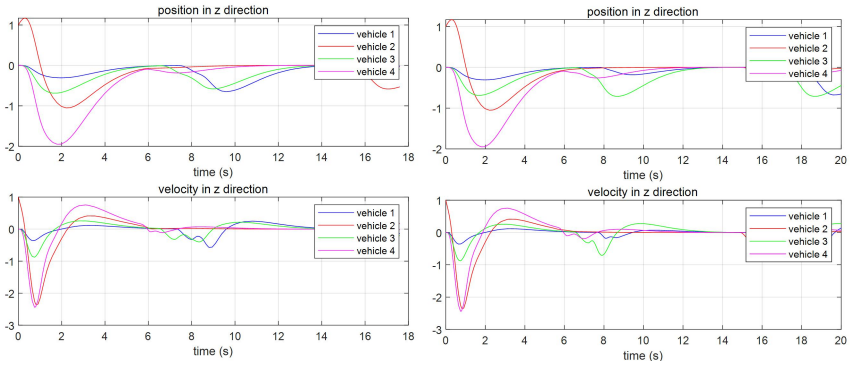

Fig. 20. z-direction position and velocity of original APF and navigation information enhanced APF 8 obstacles formation collision avoidance

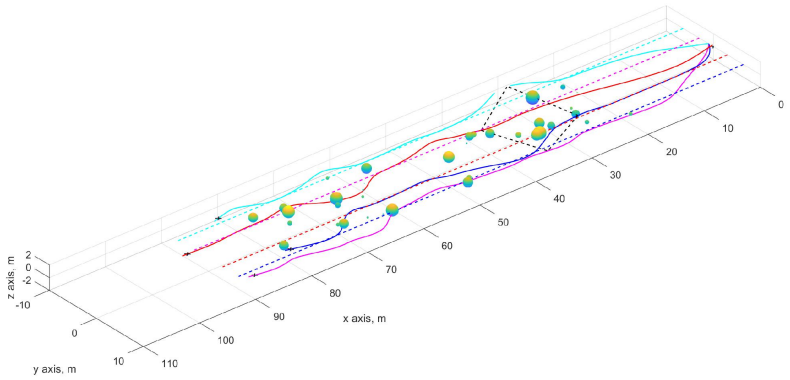

Fig. 21. The fixed safety distance APF collision avoidance trajectory with 40 obstacles

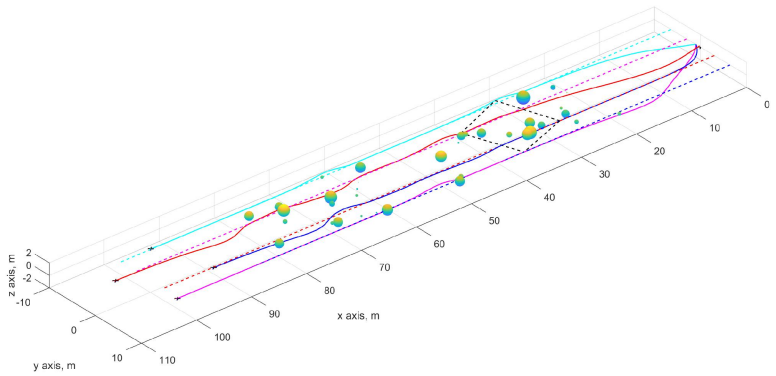

Fig. 22. The navigation information enhanced APF collision avoidance trajectory with 40 obstacles

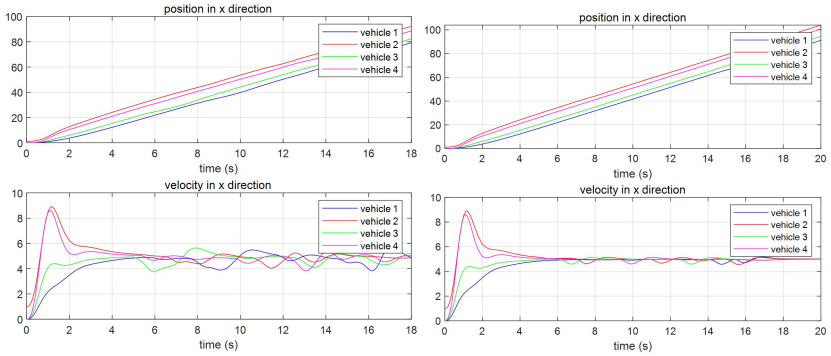

Fig. 23. x-direction position and velocity of original APF and navigation information enhanced APF 40 obstacles formation collision avoidance

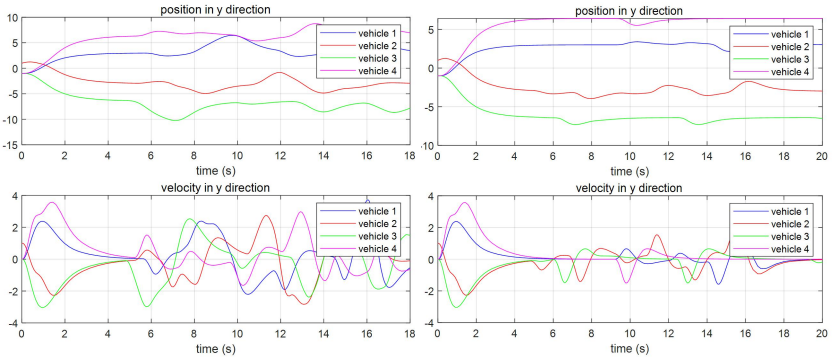

Fig. 24. y-direction position and velocity of original APF and navigation information enhanced APF 40 obstacles formation collision avoidance

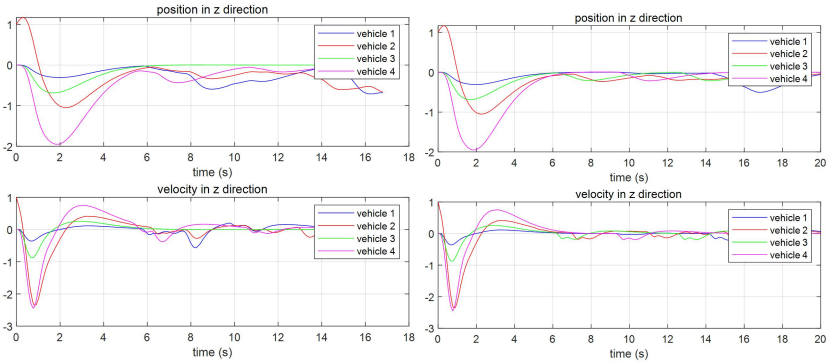

Fig. 25. z-direction position and velocity of original APF and navigation information enhanced APF 40 obstacles formation collision avoidance

The simulation of the fixed safety distance APF formation obstacle avoidance fly path is shown in Fig. 16 and Fig. 21, the uncertainty of navigation information leads to the formation's failure to avoid obstacles in time, which leads to collision. Compared with that, it can be seen from the Fig. 17 and Fig. 22 that after augmenting the APF algorithm with UAV navigation information, the potential risk caused by navigation quality uncertainty can be mitigated, the path becomes smoother. And the formation can achieve obstacle avoidance formation flight with faster response and smaller fluctuations.

5 Conclusion

This paper proposes a Navigation Information Augmented APF (NAPF) collision avoidance formation method which accounts for the uncertainty of navigation information in urban environments. The four UAV cooperative formation control strategy is obtained utilizing the virtual structure formation motion synchronization method with a corresponding Linear-Quadratic-Regulator controller. Based on this, APF is utilized to achieve formation collision avoidance. More importantly, the parameters of APF function is adaptively estimated, using the variance of navigation information and user-defined confidence probability. Simulations verify the feasibility of performing safe and effective collision avoidance for cooperative square formation flight in urban GNSS challenged environment by improved artificial potential field formation method.

References

[1] Otto, A., Agatz, N., Campbell, J., Golden, B., Pesch, E (2018) Optimization approaches for civil applications of unmanned aerial vehicles (UAVs) or aerial drones. A survey, In Networks 72-85.

[2] Mohta, Kartik, Watterson, Michael, Mulgaonkar, Yash et al (2018) Fast autonomous flight in GPS-denied and cluttered environments. In Journal Field Robotics 35:101-120.

[3] Hassa M., Abdelkefifi A. (2017) Classifications, applications, and design challenges of drones. A review, In Progress in Aerospace Sciences 91:99-131.

[4] Gennaro, Maria Carmela De, A. Jadbabaie (2006) Formation control for a cooperative multi-agent system using decentralized navigation functions. In American Control Conference. doi:10.1109/ACC.2006.1656404.

[5] Norman Li, Hugh Liu, H (2009) Multiple UAVs Formation Flight Experiments Using Virtual Structure and Motion Synchronization. AIAA Guidance, Navigation, and Control Conference. doi:10.2514/6.2009-5887.

[6] K. Kumar (2006) Review on dynamics and control of satellite systems. Journal of Spacecraft and Rockets 43:705-720.

[7] Cledat, E., D. A. Cucc (2017) Mapping GNSS Restricted Environments with a Drone Tandem and Indirect Position Control. In ISPRS Annals of Photogrammetry, Remote Sensing and Spatial Information Sciences 10:51-59.

[8] Norman H M Li, Hugh H T Liu (2009) Multiple UAVs Formation Flight Experiments Using Virtual Structure and Motion Synchronization. Modern Information Technology. doi:10.2514/6.2009-5887.

[9] H Liu, Hugh, B Zhu (2018) Formation Control of Multiple Autonomous Vehicle Systems. Formation Control of Aerial Systems. doi:10.1002/9781119263081.

[10] Ko N Y, Lee B HKo, Nak Yong, B. H. Lee (1996) Avoid-ability measure in moving obstacle avoidance problem and its use for robot motion planning. IEEE/RSJ International Conference on Intelligent Robots & Systems. doi:10.1109/IROS.1996.568984.

[11] Enchao L U, Wanxu Z (2013) Path planning for mobile robot based on improved Artificial Potential Field method in complex environment. Computer Engineering & Applications 49(24):45-48.

[12] Elbanhawi, M. et al (2017) Enabling technologies for autonomous MAV operations. In Progress in Aerospace Sciences 91:27-52.

[13] Khatib O. et al (1986) The Potential Field Approach and Operational Space Formulation in Robot Control. In Narendra K.S. (eds) Adaptive and Learning Systems 9:90-98. doi:10.1007/978-1-4757-1895-9_26.
[14] LYU Yong-shen, LIU Li-jia, YANG Xue-rong et al (2019) Formation control of UAV swarm combining artificial potential field and virtual structure. Flight Dynamics 37(03):43-47. doi:10.13645/j.cnki.f.d.20190123.001.
[15] Santana, L. Vago, A. S. BrandaO, Sarcinelli-Filho, M´ario. (2016) Navigation and Cooperative Control Using the AR.Drone Quadrotor. In Journal of Intelligent Robotic Systems 84:1-4,327-350.
[16] Belkheiri M, Rabhi A, Hajjaji A E et al (2012) Different linearization control techniques for a quadrotor system. International Conference on Communications, Computing & Control Applications. doi:10.1109/CCCA.2012.6417914.
[17] Shan J, Liu H T (2005) Close-Formation Flight Control with Motion Synchronization. Journal of Guidance, Control, and Dynamics 28(6):1316-1320.
[18] L. Qian, H. H. T. Liu (2019) Path-Following Control of A Quadrotor UAV With A Cable-Suspended Payload Under Wind Disturbances. In IEEE Transactions on Industrial Electronics 67(3):2021-2029. doi: 10.1109/TIE.2019.2905811.
[19] Shan J, Liu H H T (2006) Synchronized tracking control of multiple flying wings. American Control Conference doi:10.1109/ACC.2006.1656419.
[20] Renke He, Ruixuan Wei, Qirui Zhang (2017) UAV autonomous collision avoidance approach. Automatika 58(2):195-204.
[21] Pozna C, Troester F, Precup R E, et al (2009) On the design of an obstacle avoiding trajectory: Method and simulation. Mathematics and Computers in Simulation 79(7):2211-2226.
[22] Enchao L U, Wanxu Z (2013) Path planning for mobile robot based on improved Artificial Potential Field method in complex environment. Computer Engineering & Applications 49(24):45-48.
[23] Liu Z X, Yang L X, Wang J G (2012) Soccer Robot Path Planning Based on Evolutionary Artificial Field. Advanced Materials Research 562-564:955-958.
[24] Guo K, Qiu Z, Meng W et al (2017) Ultra-wide band based cooperative relative localization algorithm and experiments for multiple unmanned aerial vehicles in GPS denied environments. In International Journal of Micro Air Vehicles 9(3):169-186.
[25] Amedeo, Vetrella et al (2016) Differential GNSS and Vision-Based Tracking to Improve Navigation Performance in Cooperative Multi-UAV Systems. Sensors 2164-2175.